Reactive Trajectory Generation in an Unknown Environment

Kenan Cole, Adam M. Wickenheiser

Abstract—**Autonomous trajectory generation for unmanned aerial vehicles (UAVs) in unknown environments continues to be an important research area as UAVs become more prolific. In this paper, we develop a trajectory generation algorithm for a vehicle in an unknown environment with wind disturbances, that relies only on the vehicle's on-board distance sensors and communication with other vehicles within a finite region to generate a collision-free trajectory that is continuous up to the fourth derivative. The proposed trajectory generation algorithm can be used in conjunction with high-level planners and low-level motion controllers, as demonstrated. The algorithm provides guarantees that the trajectory does not violate the vehicle's thrust limitation, sensor constraints, or a user-defined clearance radius around other vehicles and obstacles. Simulation results of a quadrotor moving through an unknown environment with moving obstacles demonstrates the trajectory generation performance.**

I. Introduction

The push for autonomous and beyond-line-of-sight (BLOS) operation of UAVs is becoming more of a reality with improved sensors both commercially [1] and academically [2]. Our research examines formations of vehicles operating in unknown environments where the vehicles may be required to move relative to or independent of one another. Collision-free trajectory generation to a goal position for each vehicle is the focus of this paper.

There are several approaches for trajectory generation in the presence of obstacles and/or vehicles, including global planners, local and reactive planners, and formation controllers. Global optimization techniques are prevalent [3], [4], [5] because they can ensure convergence on the goal position, assuming a known environment. This is not possible for applications where the environment is dynamic and unknown.

Local planners examine a shorter time window to reduce the computational expense and can address ob-

Kenan Cole is a graduate student in the Mechanical and Aerospace Engineering Department, The George Washington University, Washington, DC 20052, USA

Adam M. Wickenheiser is an assistant professor in the Mechanical and Aerospace Engineering Department, The George Washington University, Washington, DC 20052, USA

stacles that may not be known a priori [6], [7]. One of the main drawbacks to the local planners is the lack of an overall safety or convergence guarantee since the optimization is occurring for short time windows for only the closest obstacles.

Reactive controllers, which are a type of local planner, employ algorithms that generate the trajectory directly as the environment is sensed [8], [9], [10]. One drawback is that they do not guarantee smoothness of the trajectory. This is problematic because vehicle thrust constraints may be violated and higher derivatives may not be bounded, which can violate vehicle controller requirements.

Formation controllers can provide solutions for collision avoidance with other vehicles in a variety of ways including global optimization where the environment must be known [11], [12] or potential fields to guide the vehicles [13]. In some cases avoidance is achieved by navigating the entire formation around the obstacle(s) [14], [15], [6]. For the present scenario, the formation can be of varying size and distribution, which is more similar to swarming behavior such as [16], which does not discuss obstacle avoidance, or [17], which relies on a distributed optimization to avoid obstacles and maintain the formation. In our scenario we seek to use the same trajectory generation for vehicles that have been re-tasked and are no longer part of the formation, so the avoidance must be applicable to obstacles and vehicles alike.

In addition to collision avoidance, the vehicle's physical limitations such as sensor range ([9], [8], [18]), maximum velocity ([10], [9]), clearance radius ([6], [10], [18], [8]), and turning rate ([18], [8]) must be considered. All of these constraints impact the generation of a feasible trajectory, and to date, no trajectory planner accounts for all of these constraints simultaneously.

Similarly, none of the cases examined consider the disturbance as input to the trajectory generation. Disturbance inclusion is much more prevalent in vehicle controllers to show ultimate bounded or asymptotic stability [19], [20], [21], [22]. In order to achieve these stability guarantees though, the controllers require that

the desired trajectory higher derivatives exist and are bounded. To meet these criteria, the control authority to overcome the disturbance must also be considered.

Our goal is to address each of these areas: collision avoidance in unknown environments, smooth trajectories (and derivatives) that do not violate vehicle thrust or sensor constraints, inclusion of the bounded disturbance, and setting maximum velocity bounds. The problem definition, properties, and assumptions are given in Sec. II. The trajectory generation is defined in Sec. III, describing the identification of potential collisions and the algorithm to adjust heading/velocity to clear the obstacle. Section IV provides the analysis for solving the trajectory curve timespan and bounding the vehicle's maximum safe cruise velocity. Section V defines the vehicle dynamics and controller for the simulation case study presented in Sec. VI. Finally Sec. VII provides concluding remarks.

II. PROBLEM DEFINITION

We define a trajectory generation algorithm with the following properties and assumptions for an environment similar to Fig. 1.

A. Algorithm Properties

Property 1: Generation of a smooth desired trajectory $\mathbf{p}_d \in \mathbb{R}^3$ where $\mathbf{p}_d^{(i)} \in \mathbb{R}^3$, $\forall i = 0, 1, \ldots, n$ exist, are bounded, and respect the vehicle's maximum thrust, f_{max}, for a translational disturbance of unknown direction and bounded magnitude, $||\mathbf{d}_p|| \leq d_{p,max}$.

Property 2: Clearance of all obstacles and vehicles by a user-defined clearance radius, r_c, which takes into account vehicle size, and measurement, estimation, and tracking errors.

B. Algorithm Assumptions

Assumption 1: Vehicle desired trajectories and obstacle motions are planar, but vehicle dynamics are not restricted to be planar.

Assumption 2: Vehicles are finite in number and heterogeneous in physical parameters (mass, max thrust, etc) and importance (i.e. higher valued asset).

Assumption 3: Vehicles sensor and communication sample periods, $\Delta T_s = \Delta T_a$, and ranges, $r_s = r_a$ are finite, equal, and provide perfect information.

Assumption 4: Vehicles share current position and heading information when in range using wireless communications.

Assumption 5: Wind disturbances are bounded, time-varying, and planar.
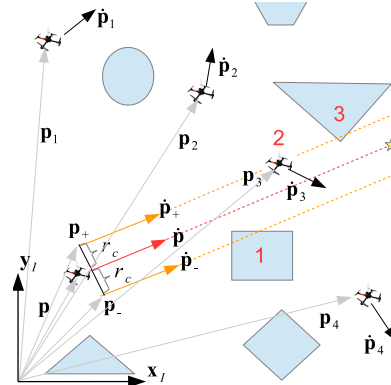
Fig. 1. Representative environment where a vehicle must navigate around other vehicles and obstacles to reach a goal position (yellow star). Two offset vectors, $\mathbf{p}_+$ and $\mathbf{p}_-$ are shown to account for the desired clearance radius, r_c. The vehicle prioritizes the potential collisions based on distance and heading angle.

Assumption 6: The clearance radius r_c ensures there are no aerodynamic interactions between one vehicle and another or with obstacles.

Assumption 7: The obstacles are of finite size and number, in plane, and move with constant velocity (less than vehicle velocity) and heading. The obstacle separation does not prevent the vehicles from moving between them.

Assumption 8: Goal positions are not too close to obstacles or each other to violate vehicle clearance radii and are not infinitely far from the coordinate origin.

III. TRAJECTORY GENERATION

The trajectory generation algorithm starts with the vehicle either at rest or heading towards the goal, $\mathbf{p}_g$, at maximum cruise velocity, v_c (see Sec. IV). As the vehicle moves in the environment, it compiles its sensor inputs to determine the most imminent threats to safety and smoothly adjusts heading and/or velocity accordingly. The vehicle only makes velocity adjustments when there are potentially both vehicle and obstacle collisions.

A. Ranking Vehicles' Maneuverability

When two or more vehicles come within communication range of each other, they exchanges cruise velocity, v_c, information to determine which vehicles maneuver and which vehicles stay on course. In accordance with Assumption 7, vehicles with larger v_c maneuver around vehicles with smaller v_c. If the vehicles have the same v_c, then the vehicles are ranked by ID. Lower ID values maneuver around vehicles with higher ID values, forming the set $ID_{mnvr} \subseteq ID_{near}$, where $ID_{near} = [ID_1 \cdots ID_m]$ is the set of all vehicles within r_a.

B. Obstacle and vehicle collision identification

The vehicle uses distance and angle to determine the most imminent threats to safety. We assume that the sensor provides information equally in all directions. The sensor output is a matrix of angles (relative to vehicle heading) and distances to nearby obstacles. The sensor scan information is used to distinguish different obstacles, each of which is given a unique identifier, ID, by the vehicle. The details of that algorithm are not presented here, but the algorithm looks at discontinuities in range and angle to separate the obstacles.

The inter-vehicle communications provide coordinate positions, $\mathbf{p}_j$, velocity, $\dot{\mathbf{p}}_j$, max cruise velocity, v_c, and ID. The information from the sensor and vehicles is combined in one matrix, $\mathbf{O}$, that tabulates the heading and distance to all the sensed obstacle points and all vehicles in ID_{mnvr}. Equation 1 defines $\mathbf{O}$, where other vehicles and obstacles are both treated as obstacles:

$$\mathbf{O} = \begin{bmatrix} \theta_1 & r_1 & ID_1 \\ \vdots & \vdots & \vdots \\ \theta_{n_1} & r_{n_1} & ID_1 \\ \vdots & \vdots & \vdots \\ \theta_{n_1+\cdots+n_{k-1}+1} & r_{n_1+\cdots+n_{k-1}+1} & ID_k \\ \vdots & \vdots & \vdots \\ \theta_{n_1+\cdots+n_k} & r_{n_1+\cdots+n_k} & ID_k \end{bmatrix} \quad (1)$$

To determine if there are obstacles along its current heading that violate r_c, the vehicle generates two offset vectors parallel to $\dot{\mathbf{p}}$, as shown in Fig. 1. The relative heading angles to the sensed points from these offset vectors are added to $\mathbf{O}$ to generate $\mathbf{O}_{aug}$:

$$\mathbf{O}_{aug} = \begin{bmatrix} \mathbf{O}, & \begin{bmatrix} \theta_{+,1} & \theta_{-,1} \\ \vdots & \vdots \\ \theta_{+,n_1+\cdots+n_k} & \theta_{-,n_1+\cdots+n_k} \end{bmatrix} \end{bmatrix} \quad (2)$$

The vehicle uses $\mathbf{O}_{aug}$ to identify the IDs of the closest sensed point, ID_r, and the point most closely aligned to the current or offset heading, ID_θ.

C. Heading Change Definition

The obstacles (or vehicles) identified by ID_r and ID_θ are used to determine the heading changes. Each obstacle ID has a corresponding number of sensed points n_{ID_r} and n_{ID_θ} from Eq. 1. The analysis that follows is for both ID_r and ID_θ, but for ease of notation, the r or θ subscripts are removed.

The first determination is the circumnavigation direction, $\mathbf{z}_\phi$, which is held constant while traversing an obstacle and minimizes heading change around obstacles. It is defined as $\pm\mathbf{z}_I$ where $\mathbf{z}_I$ is the inertial frame
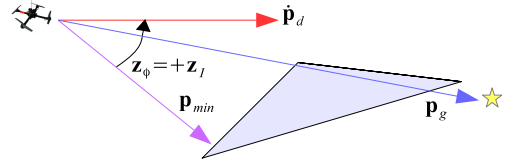
Fig. 2. Circumnavigation direction, $\mathbf{z}_\phi$, to minimize heading change.

z axis. The vehicle categorizes obstacles as "slow", $v_o \leq K_o v_c$, or "fast", $v_o > K_o v_c$ where $0 < K_o < 1$ is a user-defined variable and $v_o = ||\dot{\mathbf{p}}_o||$ is the obstacle velocity magnitude. For stationary and "slow" moving obstacles the circumnavigation direction is determined by Eq. 3 and shown in Fig. 2. For avoiding "fast" moving obstacles, the vehicle goes behind them to reduce unnecessarily lengthy maneuvers as defined in Eq. 4:

$$\mathbf{z}_{\phi,slow} = \text{sign}\left((\mathbf{p}_{min} \times \dot{\mathbf{p}}_d) \cdot \mathbf{z}_I\right) \mathbf{z}_I \quad (3)$$

$$\mathbf{z}_{\phi,fast} = \text{sign}\left((\dot{\mathbf{p}}_o \times \dot{\mathbf{p}}_d) \cdot \mathbf{z}_I\right) \mathbf{z}_I \quad (4)$$

Next, the vehicle examines the current, $\mathbf{p}_{o,i}$, and projected (if obstacle velocity has been estimated), $\mathbf{p}'_{o,i}$, obstacle positions relative to the vehicle. The projected obstacle position is given by Eq. 5 and the distances to the current and projected obstacle points is given in Eq. 6:

$$\mathbf{p}'_{o,i} = \dot{\mathbf{p}}_{o,i} \Delta T_s + \mathbf{p}_{o,i} \quad (5)$$

$$r_{i,j} = ||\mathbf{r}_{i,j}|| = ||\mathbf{p}_{o,i} - \mathbf{p}_d|| \quad (6)$$

where $i = 1, \cdots, n_{ID}$ and $j = 1, 2$. The vehicle defines the heading change as (see Fig. 3)

$$\Delta\phi_l = \begin{cases} \max\limits_{i,j} \left(\cos^{-1}\left(\frac{(\mathbf{p}_{h,i,j} - \mathbf{p}_d) \cdot \dot{\mathbf{p}}_d}{||\mathbf{p}_{h,i,j} - \mathbf{p}_d||\, ||\dot{\mathbf{p}}_d||}\right)\right), & \mathbf{z}_\phi = \mathbf{z}_I \\[2ex] \min\limits_{i,j} \left(\cos^{-1}\left(\frac{(\mathbf{p}_{h,i,j} - \mathbf{p}_d) \cdot \dot{\mathbf{p}}_d}{||\mathbf{p}_{h,i,j} - \mathbf{p}_d||\, ||\dot{\mathbf{p}}_d||}\right)\right), & \mathbf{z}_\phi = -\mathbf{z}_I \end{cases} \quad (7)$$

where $l = r, \theta$ and

$$\mathbf{p}_{h,i,j} = \mathbf{p}_d + p_{h,i,j} \mathbf{R}_{\phi_{h,i,j}} \mathbf{r}_{i,j} \quad (8)$$

$$\phi_{h,i,j} = \sin^{-1} \frac{r_c}{r_{i,j}} \quad (9)$$

$$p_{h,i,j} = \sqrt{(r_{i,j})^2 - r_c^2} \quad (10)$$

where $\mathbf{R}_{\phi_{h,i,j}}$ is the rotation matrix for a $\phi_{h,i,j}$ rotation about $\mathbf{z}_I$. The circumnavigation direction for $\Delta\phi_l$ is

$$\mathbf{z}_{\Delta\phi_l} = \text{sign}\left((\dot{\mathbf{p}}_d \times (\mathbf{p}_h - \mathbf{p}_d)) \cdot \mathbf{z}_I\right) \mathbf{z}_I \quad (11)$$

This produces two candidate heading changes, $\Delta\phi_r$ and $\Delta\phi_\theta$. The third candidate heading change is to the goal position as given by Eq. 12, where the circumnavigation direction is given by Eq. 13:

$$\Delta\phi_g = \cos^{-1}\left(\frac{(\mathbf{p}_g - \mathbf{p}_d) \cdot \dot{\mathbf{p}}_d}{||\mathbf{p}_g - \mathbf{p}_d||\, ||\dot{\mathbf{p}}_d||}\right) \quad (12)$$

$$\mathbf{z}_{\phi,g} = \text{sign}\left((\dot{\mathbf{p}}_d \times (\mathbf{p}_g - \mathbf{p}_d)) \cdot \mathbf{z}_I\right) \mathbf{z}_I \quad (13)$$
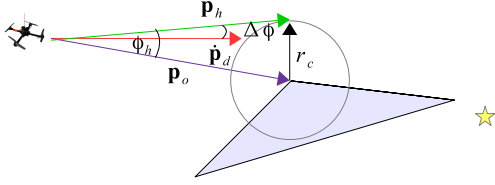
Fig. 3. Determination of $\Delta\phi$ for all the sensed obstacle points.

Fig. 4. Example heading change scenarios. (A) The circumnavigation directions are equal so the max or min can be taken. (B) Both $\Delta\phi_r$ and $\Delta\phi_\theta$ satisfy the $\Delta\phi_{min}$ and $\Delta\phi_{max}$ constraints. To minimize heading change, $\Delta\phi = \text{argmin}(|\Delta\phi_r|, |\Delta\phi_\theta|)$.

The three candidate heading changes are used to determine the actual heading change in Eq. 14, and Figure 4 shows two example cases. The conditions in Eq. 14 are evaluated in sequence.

$$\Delta\phi = \begin{cases} \Delta\phi_g, & ||\mathbf{p}_d - \mathbf{p}_g|| < \min_i(r_{i,1}) \\ \max(\Delta\phi_r, \Delta\phi_\theta, \Delta\phi_g), & \mathbf{z}_{\phi,r} = \mathbf{z}_{\phi,\theta} = \mathbf{z}_I \\ \min(\Delta\phi_r, \Delta\phi_\theta, \Delta\phi_g), & \mathbf{z}_{\phi,r} = \mathbf{z}_{\phi,\theta} = -\mathbf{z}_I \\ \Delta\phi_r, & \Delta\phi_{min} > \Delta\phi_{max} \\ \Delta\phi_g, & \Delta\phi_{min} \leq \Delta\phi_g \leq \Delta\phi_{max} \\ \text{argmin}(|\Delta\phi_r|, |\Delta\phi_\theta|), & \text{otherwise} \end{cases}$$

(14)

where r_{stop} is

$$\Delta\phi_{min} = \Delta\phi_r, \quad \Delta\phi_{max} = \Delta\phi_\theta, \quad \text{for } \mathbf{z}_{\phi,r} = \mathbf{z}_I \quad (15)$$

$$\Delta\phi_{min} = \Delta\phi_\theta, \quad \Delta\phi_{max} = \Delta\phi_r, \quad \text{for } \mathbf{z}_{\phi,r} = -\mathbf{z}_I \quad (16)$$

For cases where $\mathbf{z}_{\phi,r} = \mathbf{z}_{\phi,\theta}$ and the maximum heading change corresponds to an obstacle (i.e. not other vehicles or the goal position), the vehicle also determines if an additional heading change is necessary to match its component velocity in the direction of the obstacle velocity to v_o. The vehicle uses $\Delta\phi_l$ from Eq. 7 to determine the magnitude of the vehicle velocity in the direction of the obstacle velocity, v_{vo}:

$$\dot{\mathbf{p}}_d' = \mathbf{R}_{\Delta\phi_l}\dot{\mathbf{p}}_d \quad (17)$$

$$v_{vo} = \dot{\mathbf{p}}_d' \cdot \frac{\dot{\mathbf{p}}_o}{||\dot{\mathbf{p}}_o||} \quad (18)$$

where $\mathbf{R}_{\Delta\phi_l}$ is the rotation matrix for a $\Delta\phi_l$ rotation about $\mathbf{z}_I$. If $v_{vo} < ||\dot{\mathbf{p}}_o||$ the vehicle adjusts heading by $\Delta\phi_{vo}$:

$$\Delta\phi_{vo} = \sin^{-1}\left(\frac{||\dot{\mathbf{p}}_o||}{||\dot{\mathbf{p}}_d'||}\right) - \sin^{-1}\left(\frac{v_{vo}}{||\dot{\mathbf{p}}_d'||}\right) \quad (19)$$

This heading change, $\Delta\phi_{vo}$, is then added to $\Delta\phi_l$ to produce new the candidate headings:

$$\Delta\phi_l' = (\mathbf{z}_I \cdot \mathbf{z}_{\Delta\phi_l})\Delta\phi_l + (\mathbf{z}_I \cdot \mathbf{z}_{\Delta\phi_{vo,l}})\Delta\phi_{vo,l} \quad (20)$$

where $l = r, \theta$, and the overall circumnavigation directions, $\mathbf{z}_{\phi,r}$ and $\mathbf{z}_{\phi,\theta}$, are the circumnavigation directions of the larger heading change angle, $\Delta\phi_l'$ or $\Delta\phi_{vo,l}$. The vehicle uses $\Delta\phi_l'$ in Eq. 14 for the two cases where $\mathbf{z}_{\phi,r} = \mathbf{z}_{\phi,\theta}$ to determine the final $\Delta\phi$.

D. Smooth heading and velocity transitions

The trajectory generation utilizes sigmoid functions to transition from the current heading, ϕ, and velocity, $v = ||\dot{\mathbf{p}}_d||$, to a new heading, ϕ_n, and velocity, v_n. The hyperbolic tangent function, $(\tanh)$, is chosen for its widespread use in generating smooth transitions [23]:

$$\phi = c_1\tanh(c_2\tau - c_3) + c_4 \quad (21)$$

$$v = d_1\tanh(d_2\tau - d_3) + d_4 \quad (22)$$

where c_i and d_i are coefficients to be determined and τ is the sigmoid curve time (see Sec. IV). The desired velocity vector is then

$$\dot{\mathbf{p}}_d = \begin{bmatrix} v\cos\phi \\ v\sin\phi \end{bmatrix} \quad (23)$$

The coefficients can be solved analytically by considering the following assumptions: (1) each sigmoid function occurs over the time interval $\tau = 0$ to $\tau = \tau_f$, and (2) since $\tanh$ asymptotically approaches -1 and 1, these are approximated by, $-\varepsilon_1$ and ε_1, (where we use $|\varepsilon_1| = 1 - 10^{-3}$ to minimize error ($< 1\%$) and reduce τ_f). The coefficient solutions are summarized as:

$$c_3 = d_3 = \tanh^{-1} -\varepsilon_1 = 3.8 \quad (24)$$

$$c_2 = d_2 = 2c_3/\tau_{f_n} = 7.6/\tau_{f_n} \quad (25)$$

$$c_1 = c_4 = 0.5\Delta\phi_n \quad (26)$$

$$d_1 = d_4 = 0.5\Delta v_n \quad (27)$$

The sigmoid curves are summed during navigation so that the vehicle continues to utilize the most recent sensor information. In order to respect the vehicle thrust
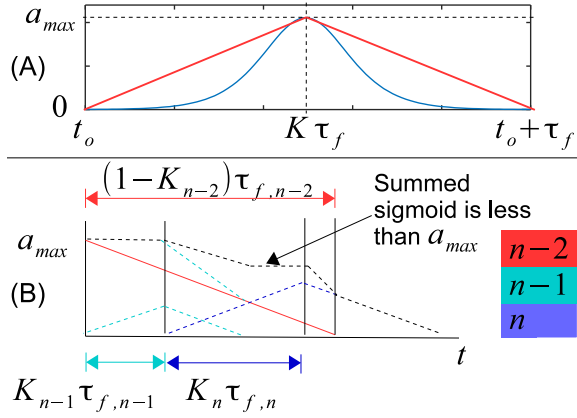
Fig. 5. (A) The sigmoid curve "slope" is approximated linearly. (B) Three sigmoid functions are summed together where the "slopes" of curves $n-1$ and n match the slope of $n-2$. The resulting function does not violate a_{max}.

limitation, successive sigmoid curves match the slope of the previous sigmoid as estimated by a linear approximation as shown in Fig. 5. This concept is further defined in Theorem 1 of Sec. IV.

IV. TRAJECTORY GUARANTEES

To guarantee the vehicle can navigate safely in the environment, we present Theorems 1 and 2, which define the sigmoid curve timespan and bound the maximum velocity, respectively.

To aid theorem development we define the available planar force (assumption 1) and the drag force:

$$f_{planar} = \sqrt{f_{max}^2 - (mg)^2} \tag{28}$$

$$\mathbf{f}_w = K_d ||\mathbf{v}_w||^2 (-\mathbf{x}_W) \tag{29}$$

$$K_d = \frac{1}{2}\rho C_D A_{x_W} \tag{30}$$

where m is the vehicle mass, g is gravity, $\mathbf{v}_w = \dot{\mathbf{p}} - \mathbf{v}_{air}$ is the resistive wind velocity between the vehicle and the air, $\mathbf{x}_W$ is the wind frame axis aligned with $\mathbf{v}_w$, ρ is the air density, C_D is the coefficient of drag, and A_{x_W} is the cross sectional area normal to the resultant drag velocity vector.

Theorem 1. *Let τ_f for the nth sigmoid be defined as*

$$\tau_{f,n} = \begin{cases} \frac{2c_3}{a_{max}}\sqrt{S_{traj}}, & t_i \geq t_{o,n-1} + \tau_{f,n-1} \\ \sqrt{\frac{2c_3\sqrt{S_{traj}}}{h_{n-1}}}, & t_i < t_{o,n-1} + \tau_{f,n-1} \end{cases} \tag{31}$$

where t_i is the current time, $t_{o,n-1}$ is the previous sigmoid curve offset (Eq. 32), h_{n-1} is the approximated linear slope of the previous sigmoid (Eq. 33), $v_{w,max} = \max(v_i, v_i + \Delta v) + v_{air}$, v_i is the current

velocity, and S_{traj} is a term of the heading and velocity change variables (Eq. 52):

$$t_{o,n} = \max(t_i, t_{o,n-1} + K_{n-1}\tau_{f,n-1}) \tag{32}$$

$$h_n = \begin{cases} \frac{a_{max}}{(1-K)\tau_{f,n}}, & t_i \geq t_{o,n-1} + \tau_{f,n-1} \\ h_{n-1}, & t_i < t_{o,n-1} + \tau_{f,n-1} \end{cases} \tag{33}$$

$$a_{max} = 1/m \left(f_{planar} - K_d v_{w,max}^2 \right) \tag{34}$$

$$S_{traj} = (c_1(d_1 H + d_4)(1 - H^2))^2 + (d_1(1 - H^2))^2 \tag{35}$$

where H is the real solution to

$$-3c_1^2 d_1^2 H^3 - 5c_1^2 d_1 d_4 H^2 + \\ (-2c_1^2 d_4^2 + d_1^2 c_1^2 - 2d_1^2)H + d_1 d_4 c_1^2 = 0 \tag{36}$$

that satisfies $|H| < \varepsilon_1$ and $K = 0.5(\tanh^{-1}(H)/c_3 + 1)$. Then, for this solution for τ_f, the vehicle trajectory does not violate f_{max} in the presence of a bounded disturbance v_{air} that satisfies $v_{air} < \sqrt{f_{planar}/K_d}$.

Proof. The sigmoid curve timespan is constrained by the vehicle's maximum thrust. The planar force is defined as

$$\mathbf{f}_{planar} = m\ddot{\mathbf{p}} + \mathbf{f}_w \tag{37}$$

where the maximum magnitude of $\mathbf{f}_{planar}$ will be when $\ddot{\mathbf{p}}$ and $\mathbf{f}_w$ are aligned. Each term will be maximized independently which gives a conservative solution for τ_f. Using Eqs. 23, 29, and 37, we write the following inequality

$$||\mathbf{f}_{planar}|| \geq m\sqrt{v^2\dot{\phi}^2 + \dot{v}^2} + K_d v_{w,max}^2 \tag{38}$$

where $v_{w,max} = \max(v_i, v_i + \Delta v) + v_{air}$, and v_i is the current velocity. The maximum acceleration from the trajectory will be where $\frac{d||\ddot{\mathbf{p}}_d||}{dt} = 0$. This is expanded as follows:

$$\frac{d||\ddot{\mathbf{p}}_d||}{dt} = 0 \tag{39}$$

$$\frac{d}{dt}\sqrt{v^2\dot{\phi}^2 + \dot{v}^2} = 0 \tag{40}$$

$$v^2\dot{\phi}\ddot{\phi} + \dot{\phi}^2 v\dot{v} + \dot{v}\ddot{v} = 0 \tag{41}$$

Equation 41 is given in terms of the heading and velocity, but since τ_f is not known the heading and velocity are also not known. We introduce two new variables, K and H, to simplify notation and facilitate a solution. First, $\tau_{max} = K\tau_f$, where $0 \leq K \leq 1$ and τ_{max} is the value of τ where $||\ddot{\mathbf{p}}_d||$ is maximum. Typically K will be around 0.5. Second, H defines the common $\tanh$ term in each sigmoid function at the maximum value. The relationships are given as follows:

$$H = \tanh(c_2\tau - c_3) = \tanh(d_2\tau - d_3) \quad (42)$$

$$= \tanh\left(\frac{2c_3}{\tau_f}K\tau_f - c_3\right) \quad (43)$$

$$= \tanh\left(c_3(2K - 1)\right) \quad (44)$$

$$K = \frac{1}{2}\left(\frac{\tanh^{-1} H}{c_3} + 1\right) \quad (45)$$

Now the sigmoid functions can be substituted into Eq. 41 and simplified as follows:

$$v^2\dot{\phi}\ddot{\phi} + \dot{\phi}^2 v\dot{v} + \dot{v}\ddot{v} = 0 \quad (46)$$

$$(d_1 H + d_4)^2 \left(c_1 c_2(1 - H^2)\right)\left(-2c_1 c_2^2 H(1 - H^2)\right) +$$
$$\left(c_1 c_2(1 - H^2)\right)^2 (d_1 H + d_4))\left(d_1 d_2(1 - H^2)\right) +$$
$$\left(d_1 d_2(1 - H^2)\right)\left(-2d_1 d_2^2 H(1 - H^2)\right) = 0 \quad (47)$$

$$-3c_1^2 d_1^2 H^3 - 5c_1^2 d_1 d_4 H^2 +$$
$$(-2c_1^2 d_4^2 + d_1^2 c_1^2 - 2d_1^2)H +$$
$$d_1 d_4 c_1^2 = 0 \quad (48)$$

The final result in Eq. 48 is a third order polynomial in H. Since all the coefficients are known, the roots can be determined. To be a solution, the roots must be real and satisfy $|H| < \varepsilon_1$.

It should also be noted that the definition for d_4 is modified from the sigmoid coefficient definition in Eq. 27 for this proof to include the current velocity

$$d_4 = v_i + \frac{1}{2}\Delta v \quad (49)$$

We now have relationships for the most aggressive part of the trajectory. Next, the drag term is considered where the maximum is:

$$v_{w,max} = \max\left(v_i, \ v_i + \Delta v\right) + v_{air} \quad (50)$$

To facilitate the solution for τ_f we also define

$$a_{max} = \frac{1}{m}\left(f_{planar} - K_d v_{w,max}^2\right) \quad (51)$$

$$S_{traj} = (c_1(d_1 H + d_4)(1 - H^2))^2 + (d_1(1 - H^2))^2 \quad (52)$$

Utilizing the solution of H from Eq. 48, the sigmoid function definitions, and Eqs. 50, 51, and 52, we re-examine Eq. 37, and make the following substitutions

$$f_{planar} \geq m\sqrt{v^2\dot{\phi}^2 + \dot{v}^2} + K_d v_{w,max}^2 \quad (53)$$

$$a_{max}^2 \geq c_2^2 S_{traj} \quad (54)$$

$$\tau_{f,n} \geq \frac{2c_3}{a_{max}}\sqrt{S_{traj}} \quad (55)$$

Equation 55 is utilized to maximize the planar thrust. It is therefore only appropriate when previous sigmoid curves have already completed. When the current sig-

moid function is being summed with previous sigmoid functions that have not yet finished, a linear approximation of the previous sigmoid curve slope is used to determine the maximum acceleration and defined as

$$h_n = \begin{cases} \frac{a_{max}}{(1-K)\tau_{f,n}}, & t_i \geq t_{o,n-1} + \tau_{f,n-1} \\ h_{n-1}, & t_i < t_{o,n-1} + \tau_{f,n-1} \end{cases} \quad (56)$$

If the current sigmoid matches the slope of the previous sigmoid, then the maximum thrust will not be exceeded. The maximum acceleration for the current sigmoid is a function of the previous sigmoid slope and $\tau_{f,n}$ and defined by

$$a_{max,n} = h_{n-1}\tau_{f,n} \quad (57)$$

Substituting Eq. 57 into Eq. 55 and simplifying produces the following

$$\tau_{f,n} \geq \frac{2c_3}{h_{n-1}\tau_{f,n}}\sqrt{S_{traj}} \quad (58)$$

$$\tau_{f,n}^2 \geq \frac{2c_3}{h_{n-1}}\sqrt{S_{traj}} \quad (59)$$

$$\tau_{f,n} \geq \sqrt{\frac{2c_3}{h_{n-1}}\sqrt{S_{traj}}} \quad (60)$$

The two solutions for $\tau_{f,n}$ are summarized in Eq. 31. $\quad\square$

Theorem 2. *Let the vehicle's maximum cruise velocity be defined as*
$$v_c = \min\left(v_{c,v}, \ v_{c,s}\right) \quad (61)$$
where $v_{c,v}$ is the minimum real, positive solution of

$$\left(\frac{m}{r_{min}} + K_d\right)v_{c,v}^2 + 2K_d v_{air} v_{c,v} + v_{air}^2 - f_{planar} = 0 \quad (62)$$

and $v_{c,s}$ is solved simultaneously with the sigmoid curve timespan, τ_f, from the following two equations:

$$\int_0^{\tau_f} v_{c,s}\sin\phi(t)dt \leq r_s - r_c - v_{o,max}\tau_f - v_{c,s}\Delta T_s \quad (63)$$

$$\tau_f = \begin{cases} \frac{c_3 m\Delta\phi_2 v_c}{f_{planar} - K_d(v_c + v_{air})^2} + \frac{1}{2}\tau_{f,1}, & 2\Delta T_s \geq \tau_{f,1} \\ \sqrt{\frac{c_3 m\tau_{f,1}\Delta\phi_2 v_c}{2(f_{planar} - K_d(v_c + v_{air})^2)}} + \frac{1}{2}\tau_{f,1}, & 2\Delta T_s < \tau_{f,1} \end{cases} \quad (64)$$

where the minimum turn radius, r_{min} is user or vehicle defined, $v_{o,max}$ is the expected maximum obstacle velocity, and

$$\Delta\phi_1 = \cos^{-1}\left(\frac{r_s - \Delta T_s(v_{o,max} - v_{c,s})}{r_s}\right) + \sin^{-1}\left(\frac{r_c}{r_s}\right) \quad (65)$$

$$\Delta\phi_2 = \pi/2 + \sin^{-1}\left(v_{o,max}/v_{c,s}\right) - \Delta\phi_1 \quad (66)$$

$$\tau_{f,1} = \frac{c_3 m\Delta\phi_1 v_{c,s}}{f_{planar} - K_d(v_{c,s} + v_{air})^2} \quad (67)$$

Then, for this solution for v_c the vehicle does not violate f_{max} when making a turn of radius $r_t \geq r_{min}$ for a bounded disturbance v_{air} applied in any direction that satisfies $v_{air} < \sqrt{f_{planar}/K_d}$.

Proof. The first constraint on v_c is due to the vehicle thrust limitations. The maximum values for each of the components in Eq. 68 are considered.

$$\mathbf{f}_d = m\mathbf{g} + \mathbf{R}_{WI}\mathbf{f}_w + \overbrace{\mathbf{f}_n + \mathbf{f}_t}^{m\ddot{\mathbf{p}}} \qquad (68)$$

The worst case drag force, $f_{w,max}$ occurs when the vehicle is traveling at v_c into the wind. Likewise, the maximum normal force occurs for the vehicle's tightest turning radius r_{min}. Finally, because the vehicle is at its maximum cruise velocity, $\mathbf{f}_{t,max} = 0$. The maximum values of each of the components are summarized in Eqs. 69 to 71.

$$f_{w,max} = \frac{1}{2}\rho C_D A_{x_W} v_{w-max}^2 = K_d v_{w-max}^2 \qquad (69)$$

$$f_{n,max} = m\frac{v_c^2}{r_{min}} \qquad (70)$$

$$f_{t,max} = 0 \qquad (71)$$

where $v_{w,max} = v_c + v_{air}$ and we assume that the area normal to x_W, A_{x_W}, and the drag coefficient, C_D are known.

The planar force vector is defined by

$$\mathbf{f}_{planar} = \mathbf{f}_n + \mathbf{f}_w \qquad (72)$$

where the maximum magnitude of $\mathbf{f}_{planar}$ occurs when $\mathbf{f}_n$ and $\mathbf{f}_w$ are aligned:

$$||\mathbf{f}_{planar}|| \geq \frac{mv_c^2}{r_{min}} + K_d\left(v_c + v_{air}\right)^2 \qquad (73)$$

Equation 73 is equivalent to Eq. 62.

Since Eq. 62 is a quadratic in v_c, we can write

$$a_{vc}v_c^2 + b_{vc}v_c + c_{vc} = 0 \qquad (74)$$

$$a_{vc} = \frac{m}{r_{min}} + K_d \qquad (75)$$

$$b_{vc} = 2K_d v_{air} \qquad (76)$$

$$c_{vc} = K_d v_{air}^2 - f_{planar} \qquad (77)$$

The roots are then

$$v_c = \frac{-b_{vc} \pm \sqrt{b_{vc}^2 - 4a_{vc}c_{vc}}}{2a_{vc}} \qquad (78)$$

The solution for v_c must be real and positive which means $b_{vc}^2 - 4a_{vc}c_{vc} \geq 0$ and $-b_{vc} + \sqrt{b_{vc}^2 - 4a_{vc}c_{vc}} > 0$. Re-arranging these two inequalities gives

$$4a_{vc}c_{vc} \leq b_{vc}^2 \qquad (79)$$

$$4a_{vc}c_{vc} < 0 \qquad (80)$$

which shows that the second inequality is the more restrictive constraint. Since $a_{vc} > 0$, Eq. 80 reduces to $c_{vc} \leq 0$. Solving for v_{air} gives

$$c_{vc} \leq 0 \qquad (81)$$

$$K_d v_{air}^2 - f_{planar} \leq 0 \qquad (82)$$

$$v_{air} \leq \sqrt{\frac{f_{planar}}{K_d}} \qquad (83)$$

The second constraint on v_c is due to sensor limitations. We consider a vehicle traveling towards an obstacle where the velocity vector of the vehicle is opposite the velocity vector of the obstacle. In the worst case scenario the vehicle is $r_s + \varepsilon$ away from the obstacle and thus does not sense it. After ΔT_s the sensor will identify the obstacle and a heading change determined. The heading change is

$$\Delta\phi_1 = \cos^{-1}\left(\frac{r_s - \Delta T_s(v_{o,max} + v_c)}{r_s}\right) + \sin^{-1}\frac{r_c}{r_s} \qquad (84)$$

After $2\Delta T_s$ the vehicle makes an estimate of the obstacle velocity and determines the remaining heading change to match the component of the vehicle velocity in the obstacle's direction to the obstacle velocity. This heading change is

$$\Delta\phi_2 = \pi/2 + \sin^{-1}\left(\frac{v_o}{v_c}\right) - \Delta\phi_1 \qquad (85)$$

Since the minimum distance between the vehicle and obstacle monotonically approaches r_c, the following inequality must hold

$$\int_0^{\tau_f} v_c \sin\phi(t)dt \leq r_s - v_{o,max}\tau_f - v_c\Delta T_s - r_c \qquad (86)$$

when Eq. 86 is re-arranged it is equivalent to Eq. 63. This equation has two unknowns in v_c and τ_f. The solution for τ_f is dependent on Eq. 31. For the initial heading change, $t \geq t_{o,n-1} + K_{n-1}\tau_{f,n-1}$ since there is no $n-1$ sigmoid curve. Additionally since $\Delta v = 0$, S_{traj} simplifies to $(c_1 d_4)^2 = (c_1 v_c)^2$. Since v_c is unknown, $a_{max} = 1/m(f_{planar} - K_d(v_c + v_{air})^2)$. Eq. 31 can be simplified as:

$$\tau_f = \frac{2c_3 mc_1 v_c}{f_{planar} - K_d(v_c + v_{air})^2} \qquad (87)$$

Substituting Eq. 26 into Eq. 87 gives the initial timespan as

$$\tau_{f,1} = \frac{c_3 m\Delta\phi_1 v_c}{f_{planar} - K_d(v_c + v_{air})^2} \qquad (88)$$

The second sigmoid heading change of $\Delta\phi_2$ will also be solved by Eq. 31, but it is unknown whether $\tau_{f,1} \geq 2\Delta T_s$. If it is not, then:

$$h_{n-1} = \frac{1/m(f_{planar} - K_d(v_c + v_{air})^2)}{1/2\tau_{f,1}} \qquad (89)$$

and the sigmoid curve timespan is defined as

$$\tau_f =$$
$$\begin{cases} \frac{c_3 m \Delta \phi_2 v_c}{f_{planar} - K_d(v_c + v_{air})^2} + \frac{1}{2}\tau_{f,1}, & 2\Delta T_s \geq \tau_{f,1} \\ \sqrt{\frac{c_3 m \tau_{f,1} \Delta \phi_2 v_c}{2(f_{planar} - K_d(v_c + v_{air})^2)}} + \frac{1}{2}\tau_{f,1}, & 2\Delta T_s < \tau_{f,1} \end{cases}$$
(90)

Equations 86 and 90 must be solved simultaneously for v_c and τ_f.

Once both constraints have been considered, the cruise velocity is the minimum value as defined by Eq. 61. □

A. Goal Position Convergence

The vehicle continues to head towards the goal position, $\mathbf{p}_g$, and once $||\dot{\mathbf{p}}_g|| = 0$, the vehicle reaches the goal position in finite time. We define $e_{\phi_g} = \phi_g - \phi$ as the error in the heading angle towards the goal position and r_g as the distance to the goal position. The following statements can be made:

1) When the vehicle starts moving it is headed towards the goal position, $e_{\phi_g} = 0$, and is some distance, $r_g > 0$ away.
2) The vehicle maneuvers around obstacles and other vehicles and from Assumption 7, $|e_{\phi_g}| > 0$ for a finite time. Once the obstacles have been cleared $e_{\phi_g} \to 0$ and $r_g \to 0$.

V. VEHICLE AND CONTROLLER

The vehicle dynamics for a quadrotor are given in Eqs. 91 and 92. Equation 91 is written in the inertial frame, and Eq. 92 is written in the body frame:

$$m\ddot{\mathbf{p}} = \mathbf{f} + m\mathbf{g} + \mathbf{d}_p \tag{91}$$
$$\mathbf{J}\dot{\omega} = \omega \times \mathbf{J}\omega + \mathbf{u} + \mathbf{R}_{IB}\mathbf{d}_\omega \tag{92}$$

where $\mathbf{f}$ is the total thrust, $\mathbf{d}_p$ is the translational disturbance (including drag), $\mathbf{J}$ is the vehicle moment of inertia, $\dot{\omega}$ is the rotational acceleration, $\mathbf{u}$ is the total torque, $\mathbf{R}_{IB}$ is the rotation matrix from the inertial to body frame, and $\mathbf{d}_\omega$ is the rotational disturbance. The control inputs are the vehicle force, $\mathbf{f}$, and torque, $\mathbf{u}$.

The vehicle dynamics also include aerodynamic effects on the propellers like thrust reduction from propeller inflow velocity [24] and blade flapping [25].

The vehicle controller uses an inner- and outer-loop control similar to [26], [27] where the outer loop controls translation and the inner loop controls rotation. The outer loop uses a nonlinear robust integral of the sign of the error (RISE) controller [22] (Eqs. 93 to 95) and the inner loop uses PID control [27] (Eq. 96):

$$\mathbf{f} = (k_s + 1)\mathbf{e}_2 - (k_s + 1)\mathbf{e}_2(0) + \nu \tag{93}$$
$$\dot{\nu} = (k_s + 1)\alpha_2\mathbf{e}_2 + \beta\text{sign}(\mathbf{e}_2) \tag{94}$$
$$\mathbf{e}_2 = \dot{\mathbf{e}}_1 + \alpha_1(\mathbf{p}_d - \mathbf{p}) \tag{95}$$
$$\mathbf{u} = k_p\mathbf{q}_d + k_i \int \mathbf{q}_d dt + k_d\dot{\mathbf{q}}_\mathbf{d} \tag{96}$$

where $k_s > 0$ and $\alpha_2 > 1/2$ are translational control gains, and $k_p, k_i, k_d > 0$ are PID control gains for desired Euler angles, $\mathbf{q}_d$, determined from $\mathbf{f}$.

VI. SIMULATION RESULTS

To demonstrate the algorithm capabilities, we show a scenario where two vehicles navigate into a building to different goal positions. There is a bounded mean wind disturbance of 2 m/s outside the building, a transition zone on entering the building, and no wind inside. The wind field uses the Von Kármán power spectral density and is spatially correlated [28]. Both vehicles have the same parameters: $f_{max} = 10.2$N, $m = 0.54$kg, $J = \text{diag}([0.0017, 0.0017, 0.0031])$ kg/m^2, $C_d = 1.7$, $r_s = 10$m, $\Delta T_s = 1$s, $r_c = 2$m, and $A_{x_w} = 0.2$m^2. The maximum cruise velocity for both vehicles is solved from Theorem 2 as $v_c = 1.83$ m/s, and from Sec. III-A vehicle 1 maneuvers around vehicle 2. Figure 6 shows an overview of the vehicles' trajectories, Fig. 7 shows snapshots of vehicle navigation, and Fig. 8 shows smooth heading changes.

The vehicle clears the obstacle by greater than r_c, and the thrust constraint is not violated. The computation time to take the sensor input and generate a trajectory is approximately 0.5 seconds for > 160 sensor points when run on a laptop computer (Matlab 2015b, 2.8GHz processor, 8 GB RAM). It is expected that the computation time would be significantly reduced if implemented as compiled code.

VII. CONCLUSION AND FUTURE WORK

The trajectory generator presented navigates a vehicle in an unknown environment while avoiding obstacles and other vehicles and respecting the vehicle's physical limitations. The vehicle uses its sensor and communication inputs to compute heading changes to avoid obstacles by a prescribed distance. The sigmoid functions used to transition heading and velocity provide smooth motion and incorporate the heading changes from each sensor update by matching the sigmoid slopes and summing the curves. Similarly, the vehicle incorporates the estimated wind disturbance, thrust limitations, and sensor
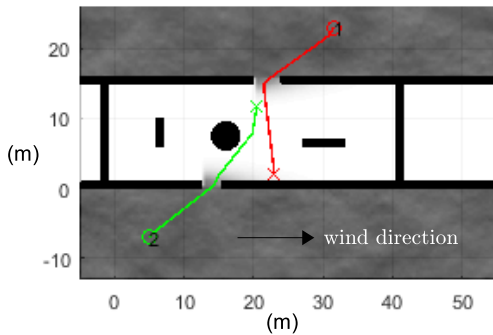
Fig. 6. Overview of vehicles moving into a building in the presence of a bounded wind disturbance (shown here at one instance in time). The vehicles clear all obstacles by r_c and do not violate f_{max}.
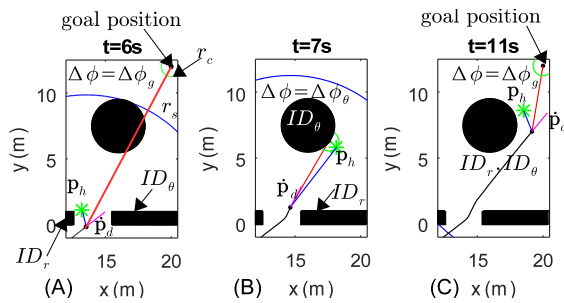
Fig. 7. Snapshots of the vehicle maneuvering in the environment. (A) The vehicle navigates through a window or door in the building. (B) The vehicle identifies the next obstacle to maneuver around. (C) The vehicle has a clear line to the goal position, safely clearing the obstacle.
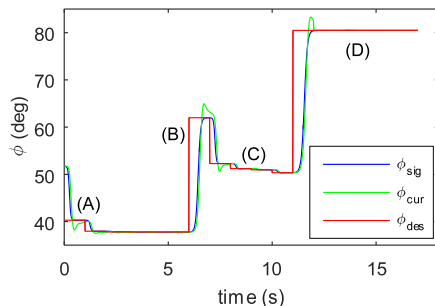
Fig. 8. Smooth heading changes for the vehicle as it navigates an unknown environment at v_c. (A) Initial adjustment on detection of the obstacle, (B) Heading change to come through the building opening (C) Heading adjustment for the circular obstacle, and (D) Heading change toward goal position.

constraints to solve for the sigmoid curve time intervals and bound the maximum safe cruise velocity. The simulation demonstrates these properties, showing smooth transitions and respecting maximum required force.

The trajectory generation presented could be extended to 3D motions by rotating the plane in which the vehicle traverses, or combining the planar motion described with a separate altitude trajectory. The thrust required for altitude adjustment could be accounted for independently, thus reducing the thrust available for planar motion. The combination of the planar and altitude trajectories would produce a 3D trajectory that respects the thrust constraints. Additional areas for exploration include relaxing the assumption of perfect sensor information, including rotational disturbances, and incorporating this trajectory generator into a higher level formation controller.

REFERENCES

[1] Echodyne. *www.echodyne.com*.
[2] L. Newmeyer, D. Wilde, B. Nelson, and M. Wirthlin. Efficient processing of phased array radar in sense and avoid application using heterogeneous computing. *26th International Conference on Field Programmable Logic and Applications*, 2016.
[3] M. Turpin, K. Mohta, N. Michael, and V. Kumar. Goal assignment and trajectory planning for large teams of interchangeable robots. *Autonomous Robots*, 2014.
[4] S. Bhattacharya, R. Ghrist, and V. Kumar. Persistent homology for path planning in uncertain environments. *IEEE Transactions on Robotics*, 2015.
[5] W. VanLoock, G. Pipeleers, M. Diehl, J. De Schutter, and J. Swevers. Optimal path following for differentially flat robotic systems through a geometric problem formulation. *IEEE Transactions on Robotics*, 2014.
[6] J. Alonso-Mora, T. Naegeli, R. Siegwart, and P. Beardsley. Collision avoidance for aerial vehicles in multi-agent scenarios. *Autonomous Robots*, 2015.
[7] Z. Shiller, S. Sharma, I. Stern, and A. Stern. Online obstacle avoidance at high speeds. *The Int. J. of Robotics Research*, 2013.
[8] J. Chunyu, Z. Qu, E. Pollak, and M. Falash. Reactive target-tracking control with obstacle avoidance of unicycle type mobile robots in a dynamic environment. *ACC, Baltimore, MD*, 2010.
[9] S.H. Tang, C.K. Ang, D. Nakhaeinia, B. Karasfi, and O. Motlagh. A reactive collision avoidance approach for mobile robot in dynamic environements. *J. of Aut. and Ctrl Eng.*, 2013.
[10] A. Matveev, M. Hoy, and A. Savkin. A globally converging algorithm for reactive robot navigation amoung moving and deforming obstacles. *Automatica*, 2015.
[11] Z. Weihua and T. Hiong Go. Robust decentralized formation flight control. *Int. J. of Aerospace Eng.*, 2011.
[12] N. Ayanian and V. Kumar. Decentralized feedback controllers for multiagent teams in environments with obstacles. *IEEE Transactions on Robotics*, 26:878–887, 2010.
[13] K. Chang, Y. Xia, and K. Huang. Coordinated formation control design with obstacle avoidance in three-dimensional space. *Journal of the Franklin Institute*, 2015.
[14] M. Zhang, Y. Shen, Q. Wang, and Y. Wang. Dynamic artificial potential field based multi robot formation control. In *IEEE Instrumentation and Measurement Technology Conference*, 2010.
[15] S. Sarkar and Kar. I.N. Formation control of multiple group of robots. *52nd IEEE Conference on Decision and Control*, 2013.
[16] C. Belta and V. Kumar. Abstraction and control for groups of robots. *IEEE Transactions on Robotics*, 2004.

[17] R. Hedjar and M. Bounkhel. Real-time obstacle avoidance for a swarm of autonomous mobile robots. *International Journal of Advanced Robotics Systems*, 2014.

[18] H. Choi, Y. Kim, and I. Hwang. Reactive collision avoidance of unmanned aerial vehicles using a single vision sensor. *Journal of Guidance, Control, and Dynamics*, 2013.

[19] D. Cabecinhas, R. Cunha, and C. Silvestre. Experimental validation of a globally stabilizing feedback controller for a quadrotor aircraft with wind disturbance rejection. In *American Control Conference, Washington, DC*, 2013.

[20] S. Waslander and C. Wang. Wind disturbance estimation and rejection for quadrotor position control. In *AIAA Unmanned Unlimited, Seattle, WA*, 2009.

[21] N. Sydney, B. Smyth, and D. Paley. Dynamic control of autonomous quadrotor flight in an esimated wind field. *IEEE Conference on Decision and Control*, 2013.

[22] N. Fischer, D. Hughes, P. Walters, E. Schwartz, and W. Dixon. Nonlinear rise-based control of an autonomous underwater vehicle. *IEEE Transactions on Robotics*, 2014.

[23] N. Fischer, A. Kan, R. Kamalapurkar, and W. Dixon. Saturated rise feedback control for a class of second-order nonlinear systems. *IEEE Transactions on Automatic Control*, 2014.

[24] G. Leishman. *Principles of Helicopter Aerodynamics*. Cambridge University Press, 2006.

[25] G. Hoffmann, H. Huang, S. Waslandar, and C. Tomlin. Quadrotor helicopter flight dynamics and control: Theory and experiment.

[26] B. Bialy, J. Klotz, K. Brink, and W.E Dixon. Lyapanov-based robust adaptive control of a quadrotor uav in the presence of modeling uncertainties. In *ACC, Washington, DC*, 2013.

[27] N. Cao and A.F. Lynch. Inner-outer loop control of a quadrotor uavs with input and state constraints. *IEEE Transactions on Control Systems Technology*, 2016.

[28] K. Cole and A. Wickenheiser. Impact of wind disturbances on vehicle station keeping and trajectory following. *AIAA Guidance, Navigation, and Control Conference, Boston, MA*, 2013.